Combustion and Flame 157 (2010) 1167–1178

Contents lists available at ScienceDirect

Combustion and Flame

journal homepage: www.elsevier.com/locate/combustflame

Ignition kernel formation and lift-off behaviour of jet-in-hot-coflow flames

E. Oldenhof *, M.J. Tummers, E.H. van Veen, D.J.E.M. Roekaerts

Department of Multi-Scale Physics, Delft University of Technology, Lorentzweg 1, 2628 CJ Delft, The Netherlands

ARTICLE INFO

Article history:
Received 28 August 2009
Received in revised form 4 January 2010
Accepted 6 January 2010
Available online 1 February 2010

Keywords:
Lift-off height
Flame stabilisation
Autoignition
Flameless combustion

ABSTRACT

The stabilisation region of turbulent non-premixed flames of natural gas mixtures burning in a hot and diluted coflow is studied by recording the flame luminescence with an intensified high-speed camera. The flame base is found to behave fundamentally differently from that of a conventional lifted jet flame in a cold air coflow. Whereas the latter flame has a sharp interface that moves up and down, ignition kernels are continuously being formed in the jet-in-hot-coflow flames, growing in size while being convected downstream. To study the lift-off height effectively given these highly variable flame structures, a new definition of lift-off height is introduced. An important parameter determining lift-off height is the mean ignition frequency density in the flame stabilisation region. An increase in coflow temperature and the addition of small quantities of higher alkanes both increase ignition frequencies, and decrease the distance between the jet exit and the location where the first ignition kernels appear. Both mechanisms lower the lift-off height. An increase in jet Reynolds number initially leads to a significant decrease of the location where ignition first occurs. Higher jet Reynolds numbers (above 5000) do not strongly alter the location of first ignition but hamper the growth of flame pockets and reduce ignition frequencies in flames with lower coflow temperatures, leading to larger lift-off heights.

© 2010 The Combustion Institute. Published by Elsevier Inc. All rights reserved.

1. Introduction

Turbulent non-premixed jet flames burning in a hot oxidiser stream containing combustion products (jet-in-hot-coflow flames) are relevant to clean combustion techniques such as flameless combustion, high-temperature air combustion (HiTAC), excess enthalpy combustion and mild combustion [1–3]. These techniques are strongly related in the sense that they all recover exhaust gas heat (for instance using regenerators or recuperators) and rely on high recirculation ratios to ensure proper mixing of one or both reactant streams with the flue gases (carrying an enthalpy deficit) before any reaction takes place. The benefits of these combustion techniques are the inherent flame stabilisation due to the high oxidiser temperature and the flat temperature profiles void of peaks, leading to low NO_x emissions. Furthermore, efficiencies are high due to the exhaust gas heat recovery.

The industrial and environmental relevance, combined with the scientific challenge of modelling these flames is the reason for the amount of attention this type of combustion has recently received in both detailed experimental [4–8] and numerical [9–14] studies on laboratory-scale setups.

An important parameter in turbulent non-premixed flames is the lift-off height. In conventional jet flames, the lift-off height, or flame stabilisation point, is the average axial height of the sharp flame interface. For jet-in-hot-coflow flames, different criteria to determine lift-off height are found in literature. Usually, a certain threshold level for an averaged quantity is defined, for instance temperature [15], OH concentration [4,16] or luminescence [17]. As gradients of average quantities in jet-in-hot-coflow flames are generally weak, specific choices of their threshold values can have great impact on the resulting value for the lift-off height. Moreover, determining the lift-off height from time-averaged fields does not reflect the complex dynamics of the lifted flame.

Several theories have been developed to explain the physical mechanisms governing lift-off for turbulent jet flames. An extensive review by Lyons [18] divides these theories and concepts in five different groups. Summarising, several theories rely on an equilibrium between flame speed and flow velocity, the flame speed being that of a laminar [19] or a turbulent [20] premixed flame, or that of a more complex 2-D flame structure [21], while other theories emphasise the competition between chemical and flow time scales [22], or the role of large-scale flow structures in transporting flame leading edges [23]. This list does not include any theory that is specific to flameless combustion. In the recent study of lift-off heights that specifically included flameless combustion [15], a generic model relating flow and chemistry time scales was used. However, it has been pointed out in several studies [6,8,24,25] that the physics of jet-in-hot-coflow flames is rather different from that of a conventional lifted jet flame. For example, Gordon et al. [8] showed by means of joint temperature, OH and CH_2O imaging the distinctly different stages of flame formation

* Corresponding author. Fax: +31 15 27 81204.
E-mail address: E.Oldenhof@tudelft.nl (E. Oldenhof).

0010-2180/$ - see front matter © 2010 The Combustion Institute. Published by Elsevier Inc. All rights reserved.
doi:10.1016/j.combustflame.2010.01.002

Nomenclature

$\langle\cdot\rangle, \bar{\cdot}$	spatial- and time averaging operators, respectively
b_1	function describing flame presence at an axial height and at an azimuthal angle in time (–)
b_2	function describing flame presence at an axial height in time (–)
d	inner diameter of the fuel jet tube (m)
$f_{ign;1}$	ignition frequency per flame surface area ($m^{-2}\,s^{-1}$)
$f_{ign;2}$	ignition frequency per axial length ($m^{-1}\,s^{-1}$)
f_{ign}	ignition frequency (1/s)
h_1	lift-off height based on b_1 (m)
h_2	lift-off height based on b_2 (m)
k_1, k_2	non-dimensional prefactors
$L_{1/2}$	distance between $z_{b;min}$ and h_2 (m)
P_{tr}	probability that an ignition event generates a burning flame at an axial distance and a time lapse (–)
P_{b1}	time averaged value of b_1 (–)
P_{b2}	time averaged value of b_2 (–)
r, z, ϕ	coordinates of the cylindrical coordinate system
tr	the value of b_2 at a distance and time lapse from an isolated ignition event
v_0	mean value of the axial velocity component with which flame pockets are transported (m/s)
v_{back}	axial velocity of the trailing edge of a projected flame pocket (m/s)
v_{front}	axial velocity of the leading edge of a projected flame pocket (m/s)
v_{jet}	bulk velocity of the jet in the fuel tube (m/s)
$v_{max;co}$	maximum velocity of the coflow (m/s)
$z_{b;min}$	the axial coordinate where ignition kernels first occur (m)
Re_{jet}	the Reynolds number of the jet, based on the bulk velocity (–)
T_{co}	temperature of the coflow (K)
$T_{max;co}$	maximum temperature of the coflow (K)
λ	Taylor length scale (m)
Φ	derivative of the expected residence time of the axial projection of a flame pocket with respect to z (s/m)

in methane jet flames in a vitiated coflow. The identified sequence started with the formation of CH_2O-rich regions, followed by the formation of small (sub-millimetre) OH-rich kernels that grow in size, rise in temperature and eventually lead to flame structures. The presence of ignition kernels has been demonstrated in other experiments, for instance in [24]. In the recent review by Mastorakos [26] an overview is given of both numerical and experimental work in the field of autoigniting flames. The combined role of chemistry and turbulence is discussed, with particular attention to the role of strain rates at mixture fraction levels most prone to autoignition, the so-called most reactive mixture fraction.

In view of these results, there appears to be a gap between experimental findings on the physical processes that are responsible for flame stabilisation in jet-in-hot-coflow flames and the conventional theories regarding lift-off height in non-premixed turbulent flames. Therefore, in this paper an attempt will be made to lay a theoretical foundation relating the lift-off height in jet-in-hot-coflow flames to the observed autoignition and convection processes. An accurate definition of lift-off height will be formulated first, and this definition will be used to compare the lift-off height of flames in the Delft Jet-in-Hot-Coflow (DJHC) burner for a range of parameters, including coflow temperature, jet fuel composition and jet Reynolds number. Secondly, the effect of these parameters on the statistics of the autoignition process will be studied in detail. The relation between the statistics and the lift-off height is then used to explain the found trends for lift-off height.

2. Experimental setup

2.1. DJHC burner

Fig. 1 shows a sketch of the upper part of the DJHC burner. This burner is designed to deliver a flame that mimics the important characteristics of flameless combustion. It creates a turbulent diffusion flame of a gaseous fuel in a coflowing oxidiser stream of high temperature carrying little oxygen. A fuel jet, emerging from a long (approximately 200 diameters) tube with an inner diameter d of 4.5 mm, develops in a coflow of hot and diluted air. This coflow is generated by a secondary burner inside an annulus with a diameter of 82.8 mm. The coflow mixture fraction can be varied, influencing both the coflow temperature and oxygen level. Due to the enthalpy deficit of the coflow (the coflow loses heat to the surroundings through radiation and convective heat transfer) the flame burns in circumstances resembling those in a furnace in flameless combustion conditions, with peak temperatures in the flame lower than those of a natural gas jet flame in normal air. The design is similar to the Adelaide JHC burner [5]. The important difference is that the secondary burner is not fully but partially premixed, which allows for seeding of the various gas flows with micron size particles that act as flow tracers in particle image velocimetry and/or laser Doppler anemometry. In this paper a z, r-coordinate system will be used with its origin at the centre of the fuel pipe exit. The z-coordinate is measured vertically upward.

2.2. Case description

Both cold-coflow flames (so-called conventional lifted flames) and hot coflow flames have been studied. The cold-coflow air has a temperature of 293 K, and a maximum mean velocity $v_{max;co}$ of 0.5 m/s. Table 1 lists the characteristics of the two different hot coflows that were considered in this study. $T_{max;co}$ represents the maximum temperature in the coflow, see Section 3.1 for further details. The coflow temperature in the DJHC-I flame is about 80 K higher than that of the DJHC-V flame. The average O_2 mass fraction in the coflow is 8.4% in the case of DJHC-I and 9.5% in the case of DJHC-V. Three different fuels were used in the central jet: Dutch

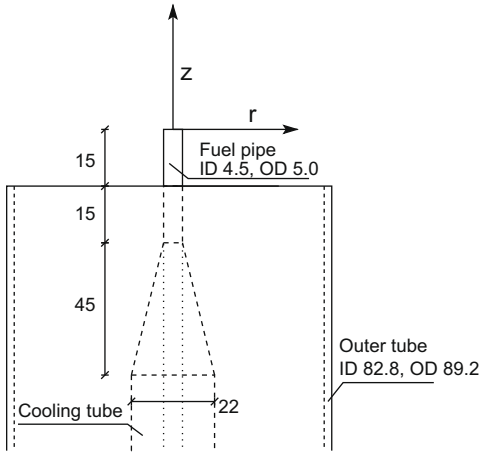

Fig. 1. Relevant dimensions of the upper part of the DJHC burner. Dimensions are in millimetres.

Table 1
Secondary burner flows and resulting maximum coflow velocity (measured with LDA) and maximum coflow temperature (measured with CARS) of the studied DJHC flames.

Case	Fuel (nl/min)	Air (nl/min)	$T_{max;co}$ (K)	$v_{max;co}$ (m/s)	$Y_{O2;co}$ (−)
DJHC-I	16.1	224	1540	4.6	8.4%
DJHC-V	15.3	231	1460	4.3	9.5%

Table 2
Compositions of the three fuels used in this study.

[Mole %]	Fuel I	Fuel II	Dutch natural gas
N_2	15.0	15.0	14.4
CH_4	85.0	81.0	81.3
C_2H_6	–	4.0	3.7
Rest	–	–	0.6

natural gas and two synthetic gases resembling Dutch natural gas, either a mixture of methane and nitrogen (fuel I) or a mixture of methane, ethane and nitrogen (fuel II), see Table 2. The jet Reynolds number was varied between 3000 and 9500, and is based on the bulk velocity in the fuel tube and the dynamic viscosity of natural gas at 300 K for the cold-coflow flames (1.14×10^{-5} Pa s) and that at 450 K for the hot-coflow flames (1.60×10^{-5} Pa s). Unlike the cold-coflow flames, the hot-coflow flames do not have to be lit externally.

2.3. Optical setup and image processing

The flame structure between $z = 0$ mm (corresponding to the fuel jet exit) and $z = 160$ mm was studied with an intensified high-speed camera (Lambert Instruments HI-CAM CR). This camera has a fibre-optically coupled two-stage intensifier with a sensitivity exceeding 50 mA/W for wavelengths between 200 nm and 550 nm. It was operated at a gate time of 400 μs. The CMOS sensor has 1280×1024 pixels, but only a quarter (1280×256) was used to achieve higher frame rates. A Nikkor UV 1:4.5, f = 105 mm lens was used, with a spectral transmission level exceeding 70% between 220 nm and 900 nm. The resolution of the resulting image is approximately 7 pixels mm^{-1}. The field of view was wide enough to capture the width of the flame up to $z \approx 130$ mm. For the jet-in-hot-coflow flames, 10^4 frames were acquired at a frame rate of 2000 fps for each case. An identical frame rate and gate time, albeit at a lower intensifier gain, was used to study the dynamics of the cold-coflow flames. To determine the lift-off heights of the cold-coflow flames, 5000 frames were taken at 200 fps, to have a larger averaging time accounting for the longer time scales involved. A background image was subtracted from each image. This background image was constructed by averaging over 1000 frames with identical exposure time, frame rate and intensification, but without the presence of a flame.

To process the images, an averaging "disc" with a radius of 8 pixels was applied after subtraction of the background image to reduce the influence of noise. Then the flame boundaries were determined based on a threshold intensity level of 8 (255 being the maximum value), making use of the built-in Matlab routine `bwboundaries.m`.[1] The dependence of the resulting lift-off height on chosen threshold values is small: within the margin of reasonable values for the threshold (flame pockets are detected as such, but noise is rejected) the difference in resulting lift-off is 3 mm.

The instantaneous leading- and trailing edge speeds of flame pockets v_{back} and v_{front} are determined from the boundary data by matching the locations of the projected edges in sequential images taken at t_n and t_{n+1}. The algorithm that determines these matches first finds candidates for the front edges at t_{n+1} from those at t_n, and selects the one with the smallest positive increment. If a front edge at t_n has multiple matches to t_{n+1}, the one with the smallest increment is selected. A front edge with no forward match has merged with the next (downstream) trailing edge, and this trailing edge is therefore also excluded as a candidate for a match with trailing edges at t_{n+1}. Front edges at t_{n+1} that have no backward match are recognised as being formed by an ignition event, and both the front edge and the trailing edge of this kernel are excluded as candidates for a match with edges at t_n. The remaining trailing edges at t_n and t_{n+1} are now matched in order of their axial location. As a result, trailing edges can have both positive and negative speeds, whereas front edge speeds are assumed to have positive speeds always. The accuracy of extracting speeds from the increments is limited by the precision with which the location of the flame boundary can be determined. This aspect has been investigated experimentally, by projecting a light dot moving on a screen, recording it with identical gain, gate time and frequency and processing the resulting images with the boundary detection routine. The resulting mean speed was found to be unbiased, as it approximates the true speed within 1%. The 95% error interval of individual measurements is estimated at ±1.1 m/s, independent of the light dot speed. It should be realised that growth speeds of ignition kernels at the moment of formation are inherently ill defined, because of the sudden increase of flame luminescence over their extents.

2.4. LDA system

LDA measurements were performed with a two-component, dual beam TSI-system. The green line (514.5 nm) and blue line (488 nm) of a 10 W Continuum Argon-ion laser were used to measure the axial and radial velocity components directly. Two of the incident beams (one of each colour) were frequency pre-shifted over 40 MHz by a Bragg cell to enable the detection of instantaneous flow reversals. The length and diameter of the measurement volume were 1.7 mm and 0.12 mm, respectively. Scattered light was collected in back-scatter mode. The photomultiplier output signals were electronically down-mixed, and subsequently collected by a FSA-3000 signal processor. All statistics were computed as transit-time weighted results to eliminate the effects of the velocity bias. Autocorrelation functions of the axial velocity component were constructed from time series with 4×10^5 velocity samples that were acquired at a mean data rate of approximately 500 Hz by using the slotting method with local normalisation [27].

2.5. CARS system

Temperatures were determined with a CARS system that has been described in detail in [28]. In a planar-boxcars phase-matching configuration, a probe volume of 700 μm length and 35 μm diameter is obtained. The single-shot imprecision of the system (one standard deviation) is 1–4% over a range from 2000 K to 300 K. The inaccuracy (the systematic error) is estimated to be 20 K. For each position in space, mean temperatures were determined from the results of 1000 single-shot CARS spectra.

3. Results and discussion

3.1. Details of the coflow

Fig. 2 shows the mean temperature field at $z = 3$ mm of the two coflows DJHC-I and DJHC-V. The coflow temperature is not constant, but depends on the radial location r.

[1] Supplementary material available, showing five snapshots before image smoothing and after smoothing, along with the detected boundaries.

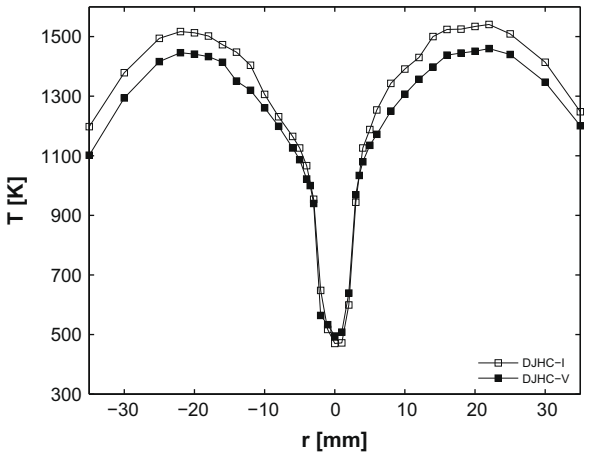

Fig. 2. Mean temperature in the DJHC-I and DJHC-V flames at $z = 3$ mm, obtained with coherent anti-Stokes Raman spectroscopy (CARS). The RMS of the coflow temperature is typically 120 K. Dutch natural gas was used in the jet stream at a jet Reynolds number of 4500.

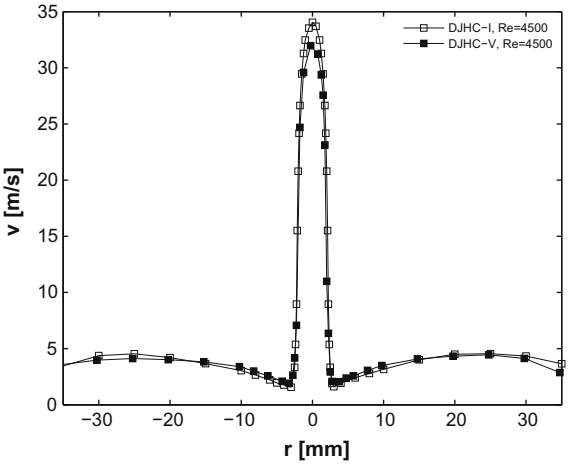

Fig. 3. Mean axial velocity in the DJHC-I and DJHC-V flames at $z = 3$ mm, obtained with laser Doppler anemometry. Dutch natural gas was used in the jet stream at a jet Reynolds number of 4500.

The velocity fields of the DJHC-I and DJHC-V flames at $z = 3$ mm are presented in Fig. 3. The larger mass flow of the DJHC-V coflow is compensated by its lower temperature and, consequently, higher density to yield nearly identical velocities.

3.2. Visual observations

Fig. 4 shows two images of the flame base of a conventional lifted jet flame (left) and the DJHC-V (right). In both cases the fuel is Dutch natural gas and $\mathrm{Re_{jet}} = 4500$. Qualitative differences between the conventional lifted flame and the jet-in-hot-coflow flame are evident. The conventional lifted flame has a sharp, connected interface with mild indentations. The jet-in-hot-coflow flame shows large spatial and temporal variations in flame interface height. Isolated flame pockets develop for $z > 80$ mm. These grow while being convected downstream where they merge thus forming a more-or-less continuous flame zone at $z \approx 120$ mm.

To study the time evolution of the pockets, the boundary detection routine mentioned earlier will be used. As an example, Fig. 5 shows three sequential luminescence images (DJHC-V, fuel II, $\mathrm{Re_{jet}} = 7000$) with the green contours indicating the boundaries

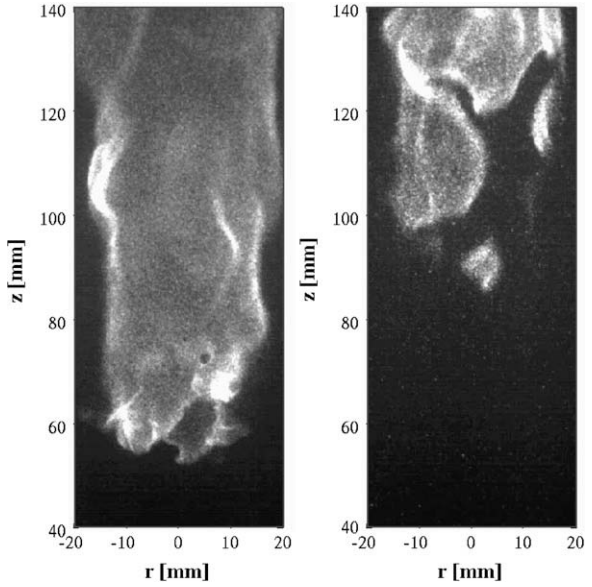

Fig. 4. Images of the flame base of a conventional lifted flame of Dutch natural gas at $\mathrm{Re_{jet}} = 4500$ (left) and of the jet-in-hot-coflow flame DJHC-V (Dutch natural gas at $\mathrm{Re_{jet}} = 4500$, right).

of detected flame pockets.[2] In the following, regions in space displaying enough luminescence to be recognised by the boundary detection routine as burning will be referred to as flame pockets. Flame pockets at their first instant of detection will be referred to as ignition kernels. The grey bars on the right of each image in Fig. 5 represent the projection of the flame pockets on the vertical coordinate axis. This one-dimensional function, referred to as $b_2(z,t)$ has logical values (zero if no flame pocket is present and one if a flame pocket is present). Most of this paper will be related to the statistics of this function in time. Although the projection on the axis leads to a loss of information, there are good reasons to study b_2 and not the two-dimensional boundary information. Most importantly, due to the axi-symmetry of the flame, the relevant ignition statistics are a function of z only. As a consequence, $b_2(z,t)$ contains all information needed to get the desired information on ignition statistics. Line-of-sight effects makes the distinction between apparently overlapping pockets impossible, as both the front and the back side of the flame are observed. However, statistics on speeds of trailing and leading edges can be acquired from $b_2(z,t)$, when edges of flame pockets occur axially separated from other flame pockets. Therefore, the essential features of the observed process, namely the formation of ignition kernels and the growth of the resulting flame pockets, can be retrieved by studying $b_2(z,t)$ alone.

The two plots in Fig. 6 show a small fraction of $b_2(z,t)$ for a jet-in-hot-coflow flame and a conventional lifted flame (cold-coflow flame). The hot-coflow flame is seen to behave very differently from the ordinary jet diffusion flame, in which a single sharp interface moves up and down. The flame pocket behaviour in the jet-in-hot-coflow flames bears the characteristics of a process of random ignition kernel formation, growth and convection.

3.3. Definition of lift-off height

The lift-off height is related to the probability of the presence of flame pockets. Two different flame probabilities are defined, P_{b1} and P_{b2}. $P_{b1}(z)$ is the probability of finding a flame pocket anywhere

[2] Supplementary content available, showing an animation of the flame DJHC-V with fuel II and $\mathrm{Re_{jet}} = 7000$ during 120 ms, slowed down by a factor of 400. The three frames shown in Fig. 5 can be seen at $t = 6.0$, 7.0 and 8.0 ms.

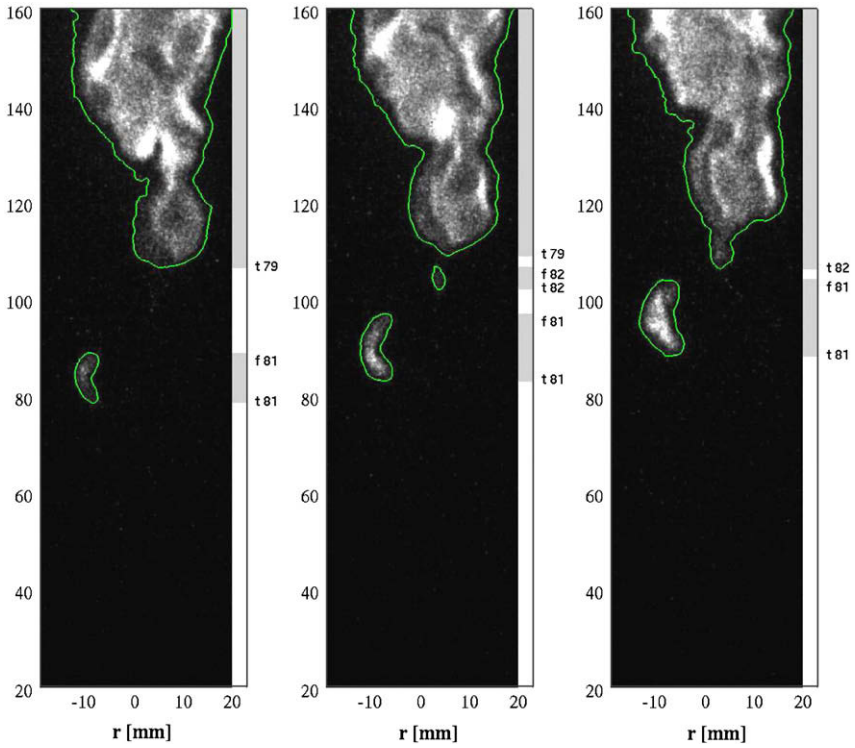

Fig. 5. Three sequential images from the case DJHC-V, fuel II, $Re_{jet} = 7000$, showing the evolution in time of the detected flame boundaries (with a 1 ms time separation, intermediate frames are removed). The bar on the right shows whether a flame pocket is present on the axial location (grey) or not (white), and the numbers indicate which trailing edges (numbers preceded by a "t") and front edges are matched by the algorithm that determines the increments, from which the projected flame speeds v_{back} and v_{front} are calculated. The new number "82" in the middle picture shows that an ignition event was recognised.

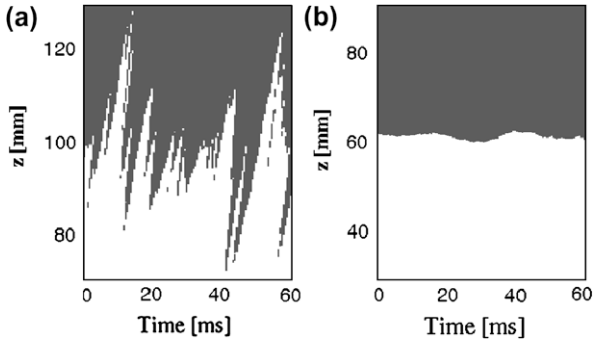

Fig. 6. The time evolution of the axial location of flame pockets $b_2(z,t)$. (a): DJHC-V, fuel II, $Re_{jet} = 5000$; (b) a lifted flame in cold coflow, Dutch natural gas, $Re_{jet} = 4500$.

on a radial line stretching outward from the burner axis, as a function of axial height. It could be determined from a planar imaging technique, such as planar laser-induced fluorescence (PLIF) by observing a radial cross-section that stretches outward from the centre and calculating the fraction of time a burning interface is found as a function of z. P_{b1} cannot be determined directly in this experimental setup, since the luminescence images result from a line-integration. However, by assuming axi-symmetry of the flame and statistical independence of the "front" and "back" of the flame, it can be reconstructed from the flame boundary observations on the centreline of the image:

$$P_{b1}(z) = 1 - (1 - P_{b1;cl}(z))^{1/2}, \quad (1)$$

where $P_{b1;cl}(z)$ is the fraction of time a pixel at height z on the centreline contains a burning pocket. The second probability $P_{b2}(z)$ is that of finding a flame pocket at a certain axial height, and is the expectation of the function $b_2(z,t)$ that was discussed in the previous section. This quantity is best visualised by drawing a horizontal line in one of the graphs in Fig. 6. P_{b2} is the fraction of the line that is in the grey region, as a function of z.

The function b_2 is equal to one whenever $b_1(\phi,z,t)$ is equal to one for an azimuthal angle ϕ, and it is as such not an azimuthally averaged property. However, studying its time evolution has a clear advantage over studying the time evolution of b_1 since it is not affected by "in-plane" transport. This enables a more rigorous analysis of the ignition and transport processes and for this reason, the focus will be primarily on b_2. In this respect, the used technique has an advantage over a planar diagnostic technique, where one cannot with certainty distinguish between true flame islands and filament-like structures being convected through the measurement plane [29], and simultaneous measurement of the velocity component into the plane is needed to interpret planar images of radicals [30].

Both probabilities P_{b1} and P_{b2} are shown in Fig. 7 for the two flames DJHC-I and DJHC-V. The lift-off height h_1 is now defined as the axial location, where P_{b1} equals 50%. A second lift-off height h_2 based on P_{b2} will also be used in the analysis. The locations corresponding to these lift-off heights are shown together with average luminescence images in Fig. 8. As expected, h_1 is located at the height where the gradient in luminescence is high. Note that in the two flames at the bottom of the picture, there is a large margin for choosing a lift-off height based on time averaged visual observations.

Figs. 9 and 10 show the lift-off heights as a function of the jet Reynolds number for the different flames. Both definitions for lift-off height yield similar trends. The minimum lift-off height $h_1 = 18d$ is found in flame DJHC-I with natural gas as fuel and at

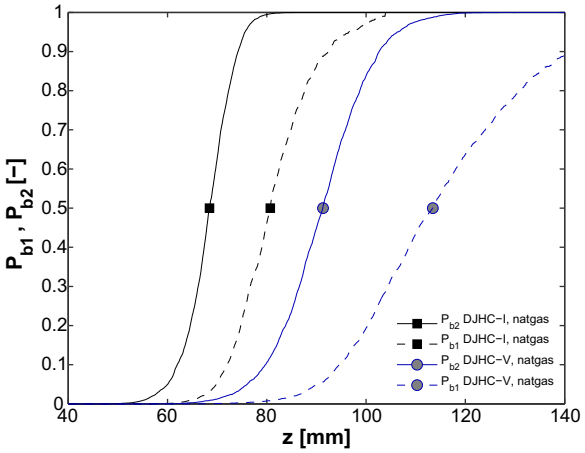

Fig. 7. The probabilities of finding a flame at an axial height on any location (P_{b2}) and at an axial height on a radial line (P_{b1}), for the DJHC-I and DJHC-V flames with natural gas, $Re_{jet} = 4500$. The symbols indicate the location, where the probabilities are 0.5.

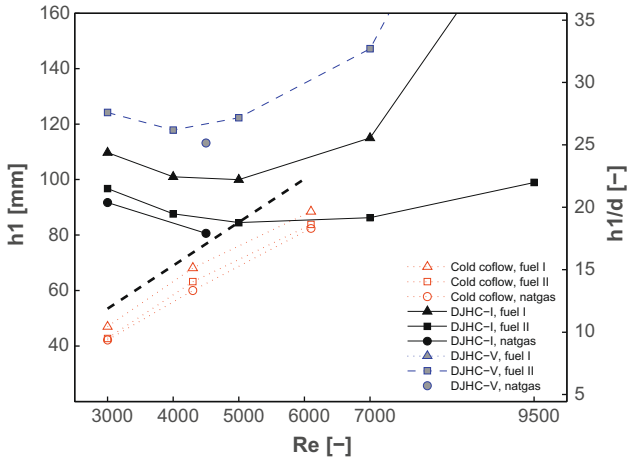

Fig. 9. Lift-off heights based on P_{b1} against jet Reynolds number. Note that the lift-off height of case DJHC-V with fuel I exceeded 160 mm for each jet Reynolds number. The thick, dashed line represents the correlation for lift-off height by Kalghatgi [20].

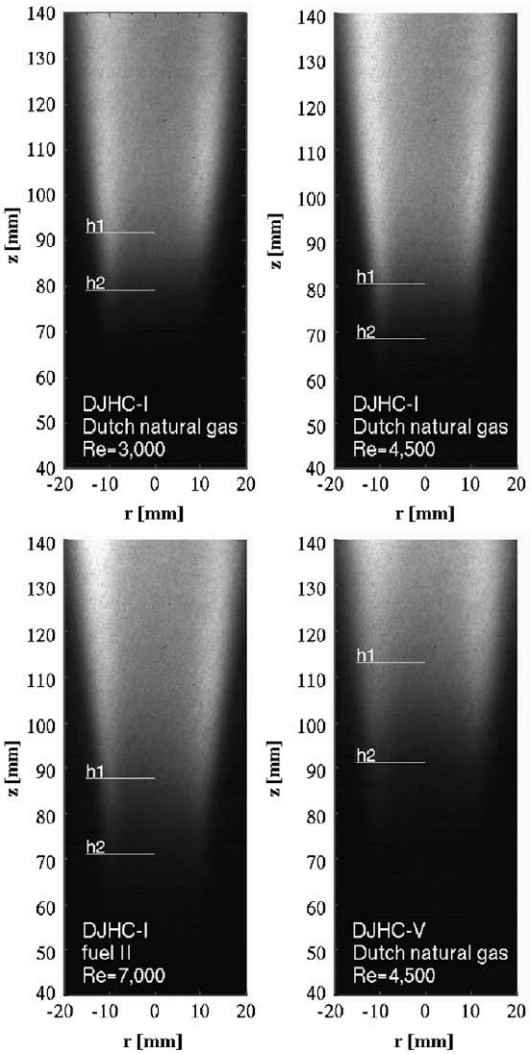

Fig. 8. The locations of $P_{b1} = 50\%$ (h_1) and of $P_{b2} = 50\%$ (h_2) marked on averaged images of four flames.

a Reynolds number of 4500. In all cases, the value of h_1 (or h_2) has a minimum at a moderate Reynolds number of approximately 5000. The value of h_2 exceeds the field of view of the camera for the flame DJHC-V with fuel I at $Re_{jet} = 9500$. This happens in several more cases for h_1, most notably in flame DJHC-V with fuel I at all Reynolds numbers. The difference between h_2 and h_1 for identical cases increases with larger Reynolds numbers. This trend will be explained in Section 3.8.

To place these results in some context, two reference cases should be mentioned. The lift-off height in the vitiated coflow burner as described in Cabra et al. [4] has been studied for a range of Reynolds numbers, with a CH_4/air fuel stream and T_{co} equal to 1350 K [17], and with an H_2/N_2 fuel stream and T_{co} equal to 1045 K [12]. The fuel jet has an inner diameter d of 4.57 mm, comparable to the 4.5 mm of the DJHC burner. In the first study, lift-off heights (based on average flame luminescence) at a coflow velocity of 4.2 m/s ranged between $h/d \approx 11$ to $h/d \approx 30$ for a jet Reynolds number ranging between 23,000 and 72,000 (v_{jet} from 80 m/s to 250 m/s), in a linear fashion. In the second study, lift-off heights ranged from $h/d \approx 3$ to $h/d \approx 20$ for a Reynolds number range of 11,000 to 35,000 (v_{jet} from 45 m/s to 160 m/s) with a coflow velocity equal to 3.5 m/s. A monotonically increasing trend was found again, with a steepening towards higher jet velocities. An initially decreasing trend as seen here has not been found in either case, the coflow temperature profile in these cases is however flat and the Reynolds numbers involved are higher.

Variation in fuel composition through the addition of higher alkanes (ethane in fuel II and propane and butane in Dutch natural gas) affects lift-off height strongly. This is in agreement with the strong influence of chemistry in jet-in-hot-coflow flames, which has been pointed out in previous numerical studies [10,31]. The results are in line with the fact that higher alkanes tend to reduce the autoignition delay times of natural gas mixtures [32].

Figs. 9 and 10 also show the lift-off behaviour of conventional jet flames for the three different fuels. In this case, the dependence of lift-off height on fuel composition is very weak. The Reynolds number dependence as indicated with the thick dashed line follows the relation of Kalghatgi [20] qualitatively, being linearly dependent on the Reynolds number. The coflow velocity of 0.5 m/s is accounted for in this calculation through the effective velocity as proposed by Montgomery et al. [33].

The issue to be addressed now is what processes cause the strong differences in lift-off height for different fuels, Reynolds numbers and coflow temperatures. For this purpose, the probability function $P_{b2}(z)$ will be studied.

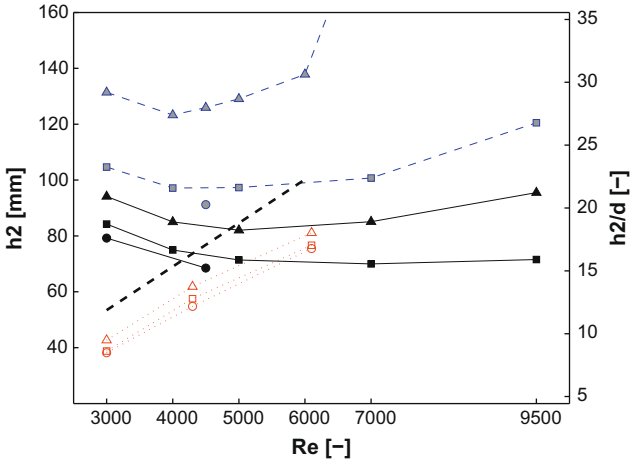

Fig. 10. Lift-off heights based on P_{b2} against jet Reynolds number. See for the legend Fig. 9.

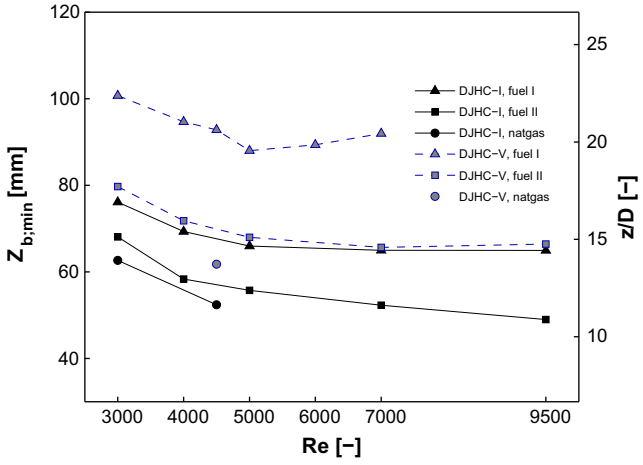

Fig. 12. The location of first ignition events $z_{b;min}$ against jet Reynolds number.

3.4. Axial location of first occurrence of autoignition kernels

Fig. 11 illustrates the influence of the jet Reynolds number on the probability P_{b2} and thus on the lift-off height h_2. It can be seen that the decrease of lift-off height for increasing Reynolds number up to $\mathrm{Re_{jet}} = 5000$ is mainly due to a horizontal shift of the curve.

The location where ignition kernels first occur, $z_{b;min}$ (arbitrarily defined as the location, where P_{b2} equals 2.5×10^{-3}), shifts downward and so does the entire curve. For higher Reynolds numbers, $z_{b;min}$ is hardly affected, but the gradient of the curve of P_{b2} decreases.

Fig. 12 illustrates the effect of coflow temperature, fuel composition and Reynolds number on $z_{b;min}$. Replacing only 4% methane by ethane (fuel II vs. fuel I) strongly decreases $z_{b;min}$, especially in DJHC-V where the coflow temperature is relatively low. The impact of increasing the jet Reynolds number is remarkable. Instead of transporting gas mixtures further away from the jet exit before autoignition due to the higher velocities, it causes $z_{b;min}$ to decrease initially in all cases. In the flame DJHC-V, with fuel I, $z_{b;min}$ rises again above $\mathrm{Re_{jet}} = 5000$, indicative of hindered formation of ignition kernels. Simply translating the axial coordinate to the residence time of a fluid parcel leads to the conclusion that autoignition delay times are reduced under the influence of increasing jet Reynolds number. Under the condition that the ignition time is larger than the typical turbulence time, faster mixing will lead to earlier generation of well-mixed spots promoting autoignition, a possibility discussed in [26]. This conclusion can however not be drawn here, because turbulence will cause variation in fluid parcel residence times at a given location. Moreover, the faster entrainment of the hotter inner part of the coflow for increasing Reynolds number is expected to play a dominant role.

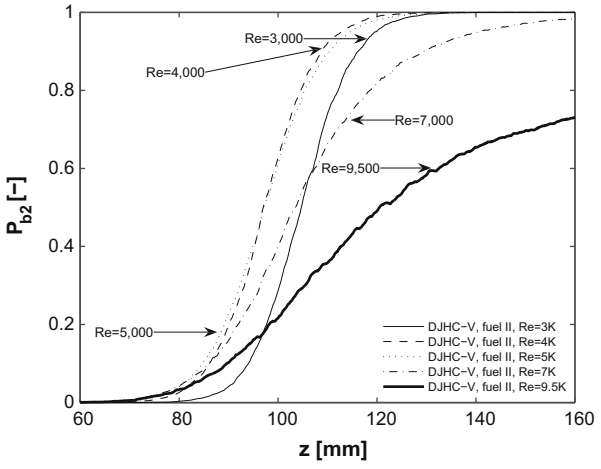

Fig. 11. The curve of P_{b2} for a range of Reynolds numbers, DJHC-V fuel II.

3.5. Transport of flame pockets

After a flame pocket has been formed, the pocket will grow while being convected downstream. Clearly, the axial velocity of the leading edge of the flame pocket v_{front} must be larger than the axial velocity of the trailing edge, v_{back}, for the axial extent of the flame pocket to increase. If flame stabilisation by flame propagation does not play a role, v_{back} should be larger than zero. The physical relevance of these velocities to the lift-off height can be demonstrated in a simple example where ignition events take place at a fixed location and at regular time intervals with frequency f_{ign}. At streamwise distances from the ignition location larger than

$$\Delta z = \left(\frac{1}{v_{\mathrm{back}}} - \frac{1}{v_{\mathrm{front}}}\right)^{-1} \frac{1}{f_{\mathrm{ign}}}, \tag{2}$$

there will be a flame at any instant in time. This illustrates that increasing v_{back} increases the lift-off height, while increasing the ignition frequency f_{ign} decreases the lift-off height.

Histograms showing the measured values of v_{back} and v_{front} of a DJHC-V flame and the trailing edge speeds of a conventional lifted flame determined by the routine as described in Section 2.3 are shown in Fig. 13. These flame speeds are not to be confused with the propagation speeds of flame structures such as studied in flat flame configurations: firstly the speed is not measured relative to its surrounding fluid, and secondly it is subject to horizontal projection. The correlation between these speeds and axial height z is very weak. As a consequence, the mean values of the pocket edge speeds can be treated to a first approximation as being independent of axial height z.

Attention will now be given to the influence of the different parameters on the mean axial flame speeds $\bar{v}_{\mathrm{front}}$ and $\bar{v}_{\mathrm{back}}$. The results for all cases are shown in Fig. 14. The effect of jet Reynolds number on $\bar{v}_{\mathrm{front}}$ is small, whereas $\bar{v}_{\mathrm{back}}$ clearly increases. This can be interpreted as a mild increase of the mean speed with which flame pockets are convected v_0, (assumed to be the average of $\bar{v}_{\mathrm{back}}$ and $\bar{v}_{\mathrm{front}}$), combined with a stronger decrease in the mean pro-

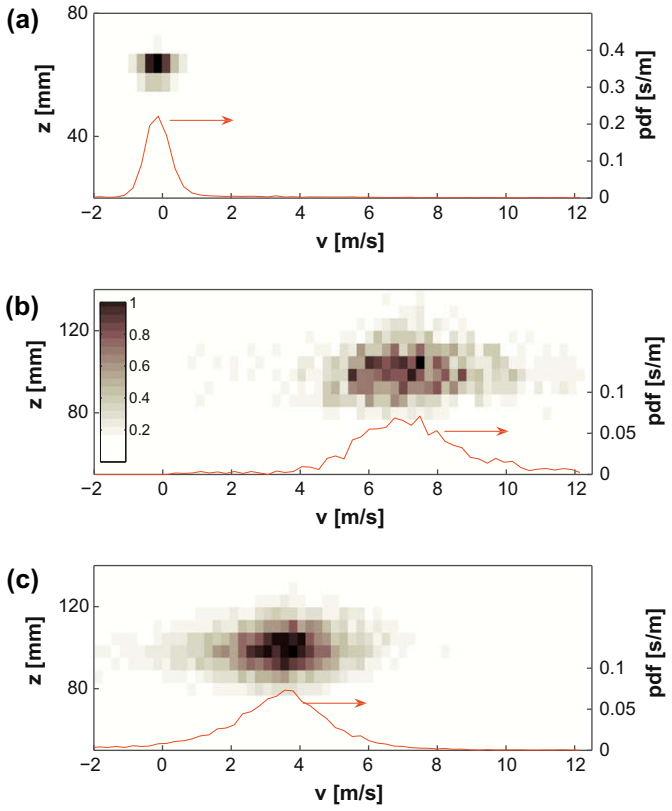

Fig. 13. Normalised 2-D histograms of velocity and location (greyscale plot) and pdfs of velocity (red line, right axis), of trailing edge in a conventional lifted flame (Dutch natural gas) (a), leading edges (b) and trailing edges (c) of flame pockets in flame DJHC-V, fuel II. The jet Reynolds number is 5000 in all cases. The 2-D histogram is normalised such that the cell with the maximum number of counts for each case gets a value equal to one.

jected flame propagation speed (the difference between $\bar{v}_{\text{back}}$ and $\bar{v}_{\text{front}}$ divided by two), for increasing jet velocity. The first trend is in agreement with the mean location of the reaction zone being near the outer edge of the jet. CARS measurements indicate that the reaction zone at $z = 120$ mm is located between $r = 13$ mm and $r = 15$ mm (case DJHC-I, $\text{Re}_{\text{jet}} = 4500$ and Dutch natural gas as fuel). Here, the mean velocity is mainly set by the coflow and is thus only mildly dependent on the jet Reynolds number. For example, the measured mean velocity at $z = 120$ mm and $r = 14$ mm increases from 5.0 m/s at a jet Reynolds number of 3000, to 6.6 m/s at $\text{Re}_{\text{jet}} = 9500$, close to the values of v_0. The location of the reaction zone also explains the lack of correlation between axial height and flame speed, as the axial gradients of mean velocity in the coflow are small. The properties of the flow field in the flame region are shown in more detail in Section 3.7. The DJHC-V flames have consistently lower projected flame propagation speeds, which might be caused by lower true flame propagation speeds or by an increase of curvature of the contours along which the flame propagates. The latter might be caused by the higher oxygen content in the coflow, increasing the stoichiometric mixture fraction and thereby moving the reaction zone closer to the shear layer of the jet.

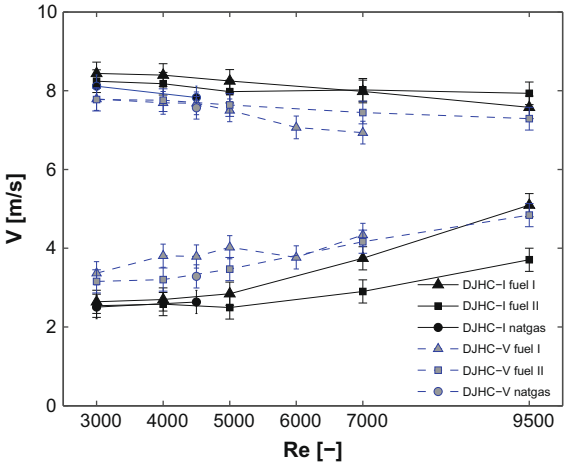

Fig. 14. Observed front- and trailing edge speeds in axial direction at different jet Reynolds numbers. Both the $\bar{v}_{\text{back}}$- and $\bar{v}_{\text{front}}$ errorbars are based on the RMS value of differences between the values obtained from the first and last set of 5000 images of their respective groups. Cases with insufficient statistics (less than 500 samples) were discarded.

3.6. Flame transfer probability

As explained in the previous section, the flame pocket growth is determined by leading and trailing edge speeds. The function that completely describes the convection, growth and possible extinction of newly formed ignition kernels is the flame transfer probability, $P_{tr}(\Delta z, \Delta t)$. This function describes the probability that an ignition event $I(z,t)$ generates a burning flame at an axial distance Δz and time lapse Δt from this event. In the case of fixed flame speeds,

$$P_{tr;\text{fixed}}(\Delta z, \Delta t) = \begin{cases} 1 & \text{if } \bar{v}_{\text{back}} \leqslant \frac{\Delta z}{\Delta t} < \bar{v}_{\text{front}} \\ 0 & \text{otherwise.} \end{cases} \tag{3}$$

This expression for P_{tr} ignores the possibility of velocity variations, or extinction, of a newly formed flame pocket. Therefore, a more refined method is needed, using $b_2(z,t)$ directly to obtain the flame transfer probability.

To demonstrate the relation between b_2 and P_{tr}, consider a single realisation of $b_2(z+\Delta z, t+\Delta t)$, conditional on an ignition event $I(z,t)$. The resulting field of $b_2(z+\Delta z, t+\Delta t)$ is the union of the field in absence of this ignition with the flame evolution of this specific ignition event, $tr(\Delta z, \Delta t)$. The expectation of b_2 (the arguments are omitted for brevity) conditional on the ignition event I follows from

$$\mathbb{E}\{b_2|\text{I}\} = \mathbb{E}\{tr\} + (1 - \mathbb{E}\{tr\})\mathbb{E}\{b2\} = P_{tr} + (1 - P_{tr})P_{\text{b2}}, \tag{4}$$

using statistical independence of the individual ignition events. Note that $\mathbb{E}$ is the "expected value" operator and "|" denotes that a conditional expectation is considered. Rewriting Eq. (4) leads to the following equation (written out fully):

$$P_{tr}(\Delta z, \Delta t) = \frac{\mathbb{E}\{b_2(z+\Delta z, t+\Delta t)|\text{I}(z,t)\} - P_{b2}(z+\Delta z)}{1 - P_{b2}(z+\Delta z)}. \tag{5}$$

In practice this means extracting samples of $b_2(z,t)$ (see Fig. 6) around a large number of ignition events accounting each time for the locally expected value of b_2 which is $P_{b2}(z+\Delta z)$. This approach works well, provided that the value of P_{b2} is not too large, and ignition events can be identified accurately. Both requirements are fulfilled by considering only ignition events at locations of low flame probability, say $P_{b2} < 0.03$. The resulting statistics consist typically of around 200 samples, with a minimum of 123 samples for the case DJHC-V with fuel I at a jet Reynolds number of 7000. Fig. 15 shows the flame transfer probability $P_{tr}(\Delta z, \Delta t)$ for four Reynolds numbers in DJHC-V flames with fuel II. These figures clearly show the mean downstream convection and growth of newly created flame pockets. The dotted blue lines according to Eq. (3) correspond well to the found flame transfer probability functions. For the

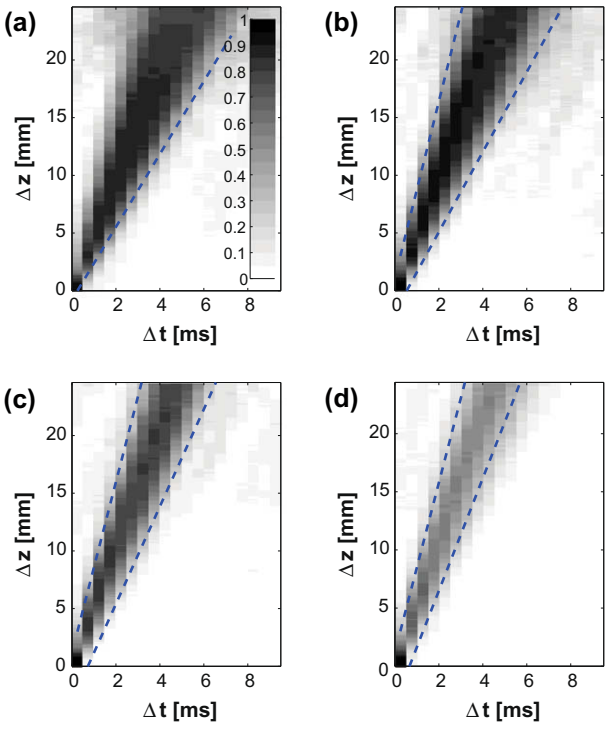

Fig. 15. The flame transfer probability P_{tr}, for flame DJHC-V, fuel II, with Reynolds number 3000 (a), 5000 (b), 7000 (c) and 9500 (d). It denotes the ensemble-averaged evolution of a flame kernel starting from its creation at $\Delta t = 0$. Each plot consists of approximately 200 of these samples. Note that at the highest Reynolds number, P_{tr} becomes more sparse, which is caused by occasional extinction events. The dotted blue lines show the pocket evolution corresponding to the values of $\bar{v}_{\text{front}}$ (steepest curve) and $\bar{v}_{\text{back}}$, as determined in Section 3.5.

highest Reynolds numbers, the effects of inhibited growth of ignition kernels and even extinction become important, as can be observed by the decrease of the transfer probability in the region between the blue dotted lines for increasing values of Δz and Δt.

The function P_{tr} acts as a convolution kernel on the ignition frequency density $f_{\text{ign};2}(z)$ (the frequency of formation of ignition kernels per unit axial length in absence of a flame) to yield the flame probability P_{b2} (with the introduction of the dummy variables z' and t'):

$$P_{b2}(z,t) = \overline{b_2} = 1 - \exp\left[-f_{\text{ign};2}(z',t') * P_{tr}(\Delta z, \Delta t)\right], \tag{6}$$

where "$*$" is the convolution operator. Therefore, the results in Fig. 15 enable the quantification of the growth of kernels and to relate ignition frequencies to the flame probability P_{b2}.

Using the time invariance of the ignition frequency, and the ansatz

$$\int P_{tr}(\Delta z, \Delta t)\,\mathrm{d}t = \Phi \Delta z, \tag{7}$$

Eq. (6) can be rewritten as a simple integral over the axial height z:

$$P_{b;2}(z) = 1 - \exp\left[-\Phi \int f_{\text{ign};2}(z')(z - z')\,\mathrm{d}z'\right]. \tag{8}$$

The parameter Φ is the derivative of the expected residence time of a projected flame pocket pertaining to an ignition event (the time between arrival of the front edge and arrival of the trailing edge) with respect to z. Note that $\Phi = 0$ implies no flame growth and hence no flame stabilisation whilst $\Phi \to \infty$ corresponds to stabilisation by flame propagation. Fig. 16 shows the time integral of P_{tr} for a range of distances from the ignition event, Δz. The assumption of linearity in Δz appears to be appropriate. The values for lower Reynolds numbers are comparable to those calculated assuming fixed flame speeds, in which case Φ simply follows from:

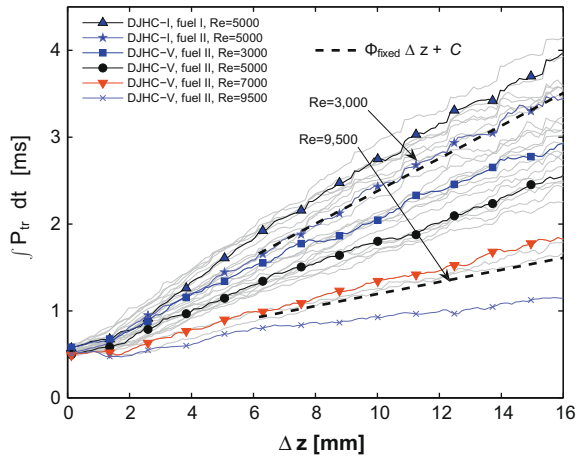

Fig. 16. The value of the time integral over P_{tr} as function of Δz, for several cases. The thick dashed black lines denote the slope based on Eqs. (7) and (9) and the flame speeds $\bar{v}_{\text{front}}$ and $\bar{v}_{\text{back}}$, of flame DJHC-V with fuel II for a jet Reynolds number of 3000 (top line) and 9500 (bottom line). The thin grey lines represent the values of all hot coflow cases, to give an impression of the amount of scatter between cases.

$$\Phi_{\text{fixed}} = \frac{1}{\bar{v}_{\text{back}}} - \frac{1}{\bar{v}_{\text{front}}}. \tag{9}$$

A characteristic of all curves is that they do not intersect the origin. This is caused by the fact that ignition kernels already have a certain size at the moment they are detected by the image processing routine. They appear as vague "streaks" of a certain size one or two frames before fully igniting and being accurately detectable. The average kernel length in axial direction upon detection is between 3 and 5 mm. This is comparable to the radius of the averaging disc (1 mm) and the convective displacement during the 400 μs exposure time (2.4 mm). Quantification of the true size of kernels at the moment of detection is therefore not undertaken here.

3.7. Ignition frequencies

The ignition frequency may be determined from the flame boundary data. However, validation of the used ignition kernel detection routine against Monte Carlo simulations showed that it was unreliable in regions, where P_{b2} has a significant value, say $P_{b2} > 0.3$, and at higher ignition frequency densities. Another shortcoming of the detection routine is that it is unable to recognise ignition events in rapid succession over small distances. An exact expression for $f_{\text{ign};2}(z)$ derived from Eq. (8) involves the second spatial derivative of P_{b2}, which results in very noisy data. The following measure for the mean ignition frequency is therefore used instead, based on the more robust quantity $\mathrm{d}P_{b2}/\mathrm{d}z$. Differentiating Eq. (8) gives

$$\left.\frac{\mathrm{d}P_{b2}}{\mathrm{d}z}\right|_{P_{b2}=1/2} = \frac{\Phi}{2} \int_0^{z(P_{b2}=1/2)} f_{\text{ign};2}\,\mathrm{d}z = \frac{\Phi}{2}(h_2 - z_{b;min})\langle f_{\text{ign};2}\rangle. \tag{10}$$

Renaming the length scale $(h_2 - z_{b;min})$ to $L_{1/2}$ gives:

$$\langle f_{\text{ign};2}\rangle = \frac{2}{\Phi\, L_{1/2}} \left.\frac{\mathrm{d}P_{b2}}{\mathrm{d}z}\right|_{P_{b2}=1/2}. \tag{11}$$

Fig. 17 shows the mean ignition frequency $\langle f_{\text{ign};2}\rangle$ as a function of jet Reynolds number for several flames. The value of $\langle f_{\text{ign};2}\rangle$ has been determined with Eq. (11) using linear fits to the curves of $P_{b2}(z)$ and those in Fig. 16 to obtain their derivatives. The ignition frequencies thus found range between 2×10^3 m^{-1} s^{-1} and 6×10^4 m^{-1}s^{-1}.

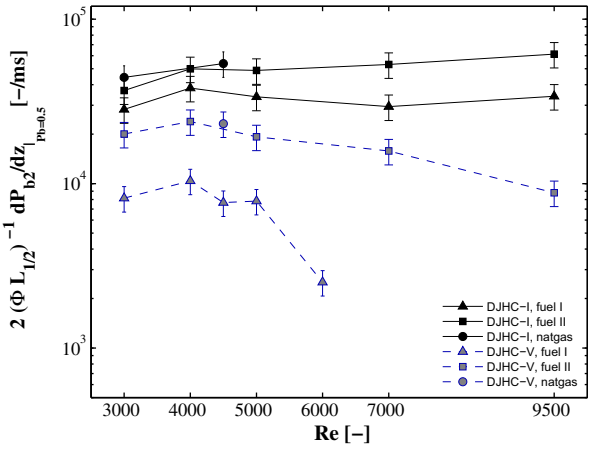

Fig. 17. Mean ignition frequency densities $\langle f_{ign;2} \rangle$ as determined with Eq. (11) against jet Reynolds number, presented on a semi-log scale.

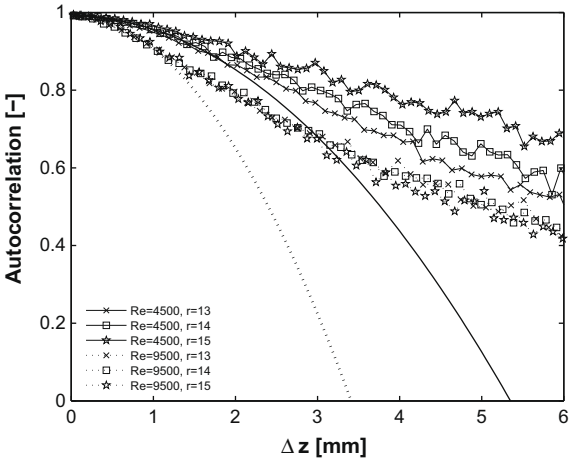

Fig. 18. Autocorrelation functions, DJHC-I, $Re_{jet} = 4500$ and $Re_{jet} = 9500$. The connected and dotted line represent the parabolic fit through the autocorrelation function at $\Delta z = 0$ for $Re_{jet} = 4500$ ($r = 14$ mm) and $Re_{jet} = 9500$ ($r = 15$ mm), respectively. These are the locations where the flame resides on average.

The average ignition frequency density calculated by the image processing routine reproduces the trends and figures for the DJHC-V flames, but the higher values are not reproduced, which is due to the shortcomings mentioned earlier. The mean ignition frequency densities of flames DJHC-I are at least two times larger than those in flames DJHC-V, and fuels with higher alkanes yield consistently higher values. The jet Reynolds number hardly has any influence on the ignition frequencies in flame DJHC-I, whereas flame DJHC-V is more sensitive to the Reynolds number, especially for fuel I.

The diminished frequency of ignition events (in DJHC-V) and increased probability of kernel extinction and limited flame pocket growth (in all cases) is expected to originate from the larger strains in the turbulent field at higher Reynolds numbers. The large role of strains on autoignition has been pointed out in previous DNS-studies [34–36]. Echekki et al. [36] showed the evolution of ignition kernels in 2-D DNS calculations with detailed hydrogen-air chemistry. A species-specific Damköhler number was introduced, and observed extinction events were related to excessive heat and species dissipation. Very recently, experimental evidence has been obtained showing that ignition kernels with super-equilibrium OH-levels strongly favour locations with low temperature gradients [37]. In order to verify that the lower ignition frequencies indeed originate from higher levels of scalar dissipation, detailed statistics on the history of the scalar field that ignition kernels experience prior to ignition would be needed, an experimental effort not undertaken in this study. However, some insight on the influence of the jet Reynolds number on the turbulent field in the reaction zone would be useful. Therefore, the quantity $(\partial u_z'/\partial z)^2$ was determined from LDA measurements by first computing the autocorrelation function (acf) of the axial velocity fluctuations and then invoking Taylor's hypothesis to convert time delay into spatial separation [38]. The resulting acfs that were measured at several radial locations in the DJHC-I flame at $z = 120$ mm for $Re_{jet} = 4500$ and $Re_{jet} = 9500$ are shown in Fig. 18.

The intercept of the parabola with the Δz-axis represents the Taylor length scale λ which is related to the strain rate as in

$$\overline{\left(\frac{\partial u'}{\partial z}\right)^2} = \frac{\overline{u'^2}}{\lambda^2}. \tag{12}$$

The resulting values for the Taylor length scale are listed in Table 3. The Taylor length scale decreases (and the variance of the velocity fluctuations increases) with increasing Reynolds number. This is clear evidence that the mean strain rate in the vicinity of the reaction zone is much larger at the higher jet Reynolds number. Both the impact of jet Reynolds numbers on ignition frequency densities in the DJHC-V flames as shown in Fig. 17 and the hindered kernel growth as was evident in Fig. 15 can therefore be linked to changes in the turbulent flow field.

Table 3
Flow characteristics in DJHC-I flames at three radial locations for $Re_{jet} = 4500$ (Dutch natural gas) and $Re_{jet} = 9500$ (fuel II). The Taylor length scales between parentheses should be addressed with some care because of the high turbulent intensity (above 30%).

	$Re_{jet} = 4500$			$Re_{jet} = 9500$		
r (mm)	13	14	15	13	14	15
$\bar{u}$ (m/s)	5.95	5.42	5.31	7.65	6.57	5.99
$\sqrt{\overline{u'^2}}/\bar{u}$ (–)	18.6%	14.8%	12.7%	31.3%	30.6%	26.4%
λ (mm)	4.8 [±0.2]	5.4 [±0.3]	5.9 [±0.3]	(3.8 [±0.2])	(3.4 [±0.2])	3.4 [±0.2]

3.8. Evaluation and implications on lift-off height

In the analysis of the mechanisms governing lift-off, the function $b_2(z,t)$ was considered to be the result of a simple stochastic process, namely that of randomly occurring local events generating infinitesimal ignition kernels with an expected flame growth that is linear in time, determined from the flame transfer probability function P_{tr}. This probability P_{tr} was assumed to be independent of the axial location z in the stabilisation region. Several deviations from the idealised process can be witnessed however. Ignition kernels do not appear as points, but as small regions in space, with a fast, but not instantaneous, transition from a non-burning to a burning state. Ignition events are unlikely to be statistically independent, as occasionally successive ignition events are witnessed in a certain region.

Although these deviations will certainly have an influence, the essential features of the flames (for instance as shown in Fig. 15) strongly resemble those of the proposed process. Stabilisation by flame propagation, which forms the basis of most theories on lift-off in turbulent non-premixed flames, as the dominant mechanism is out of the question, because the flame speed at the trailing edges is insufficient to maintain the flame base at a fixed point (see Fig. 14). This is not to say that the flame speed is irrelevant, since it affects the growth of flame pockets and thereby the lift-off height.

Until this point, the function b_2 was used to extract information on the ignition and growth statistics. The reverse direction is now

taken, showing how h_2 and h_1 depend on those statistics. Starting from Eq. (10), and taking the inverse of the gradient of P_{b2} at h_2 proportional to $L_{1/2}$, the following expression is obtained:

$$h_2 = z_{b;min} + k_2\left[\Phi\ \langle f_{ign;2}\rangle\right]^{-1/2}, \tag{13}$$

with k_2 a non-dimensional prefactor. To derive an expression for h_1, not the expected number of ignition events per time per axial length is needed, but those per time per surface area (presumably the iso-surface of the most reactive mixture fraction), because the flame propagates on a surface (the iso-surface of stoichiometry). This frequency density per surface area $f_{ign;1}$ scales as $f_{ign;2}r^{-1}$, with r the characteristic radius of the axisymmetric flame surface. As the convolution is now performed over a surface and over time (instead of over a length and over time, as in Eq. (6)), the relation between h_1 and the ignition and transport properties becomes more complex. An additional non-dimensional parameter should be introduced, for instance $\frac{v_{front}}{v_{back}}$. On dimensional grounds we therefore expect:

$$h_1 = z_{b;min} + k_1\left[\Phi\ \langle f_{ign;1}\rangle\right]^{-1/3} f\left(\frac{v_{front}}{v_{back}}\right), \tag{14}$$

with k_1 a non-dimensional prefactor. Note that, as the values of $P_{b1}(z)$ can never exceed those of $P_{b2}(z)$, h_1 must always exceed h_2. This imposes limits on the validity of Eq. (14), related to the ratio of the axial height of the considered region and the circumference of the considered flame surface. Solving the exact equation of P_{b1} for pockets growing with fixed speeds on a cylindrical surface shows that the function $f\left(\frac{v_{front}}{v_{back}}\right)$ is strictly decreasing in the part of its domain exceeding one. The trends of h_1 and h_2 as a function of jet Reynolds number – initially, both decrease by similar degree, whereas at higher jet Reynolds numbers h_1 increases much stronger than h_2-can now be understood through these arguments, as at low jet Reynolds number mainly $z_{b;min}$ is affected, whereas at higher Reynolds numbers the different scalings cause h_1 and h_2 to diverge.

4. Conclusions

By analysing high-speed recordings of luminescence in the visible and near UV-part of the spectrum, the lift-off behaviour of flames burning in a hot and diluted coflow was studied. Analysis of the luminescence images showed that the physical mechanisms governing the lift-off process in jet-in-hot-coflow flames and conventional lifted flames are very different. This difference is reflected in the trends for lift-off height as a function of jet Reynolds number, which are completely dissimilar. Instead of flame propagation, ignition kernel generation by autoignition followed by convection and growth are responsible for flame stabilisation. In order to quantify the findings, the ignition process was reduced to two parameters: the axial location where ignitions first occur $z_{b;min}$ and a mean ignition frequency density in the stabilisation region $\langle f_{ign;2}\rangle$. The axial flame growth could be described by a single parameter Φ. Based on observations and dimensional reasoning, the lift-off height follows a scaling rule as described by Eq. (14).

Addition of higher alkanes and increasing the coflow temperature have a similar effect. Both reduce the chemical timescale, leading to a lower $z_{b;min}$ and higher ignition frequencies $\langle f_{ign;2}\rangle$, reducing lift-off height. The influence of fuel composition or coflow temperature on flame pocket speeds is relatively small. The effects of jet Reynolds number on the parameters are more intricate. An increase in Reynolds number from 3000 to 5000 lowers in all cases the location of first ignition $z_{b;min}$. This is likely related to the faster entrainment of the hotter part of the coflow for increasing Reynolds numbers. An increase in jet Reynolds number leads to significantly higher mean strains of the axial velocity component at the location of the reaction zone, as shown by the decrease in the Taylor length scale. At jet Reynolds numbers exceeding 5000, this is accompanied by diminishing ignition frequencies in the flames burning in the colder coflow, while in all flames the growth of newly formed ignition kernels is hindered. Extinction of ignition kernels is occasionally witnessed at the highest Reynolds numbers. A trend seen in both $z_{b;min}$ and $\langle f_{ign;2}\rangle$, and consequently in the lift-off height, versus the jet Reynolds number is that increased levels of turbulence hinder the autoignition process more strongly in flames with slower chemistry.

Appendix A. Supplementary data

Supplementary data associated with this article can be found, in the online version, at doi:10.1016/j.combustflame.2010.01.002.

References

[1] J.A. Wünning, J.G. Wünning, Flameless oxidation to reduce thermal NO-formation, Prog. Energy Combust. Sci. 23 (1) (1997) 81–94.
[2] H. Tsuji, A.K. Gupta, T. Hasegawa, M. Katsuki, K. Kishimoto, M. Morita, High Temperature Air Combustion, CRC Press, 2003.
[3] A. Cavaliere, M. de Joannon, Mild combustion, Prog. Energy Combust. Sci. 30 (4) (2004) 329–366.
[4] R. Cabra, T. Myhrvold, J.Y. Chen, R.W. Dibble, A.N. Karpetis, R.S. Barlow, Simultaneous laser Raman–Rayleigh-lif measurements and numerical modeling results of a lifted turbulent H-2/N-2 jet flame in a vitiated coflow, Proc. Combust. Inst. 29 (2003) 1881–1888.
[5] B.B. Dally, A.N. Karpetis, R.S. Barlow, Structure of turbulent non-premixed jet flames in a diluted hot coflow, Proc. Combust. Inst. 29 (2003) 1147–1154.
[6] P.R. Medwell, P.A.M. Kalt, B.B. Dally, Simultaneous imaging of OH, formaldehyde, and temperature of turbulent non-premixed jet flames in a heated and diluted coflow, Combust. Flame 148 (1–2) (2007) 48–61.
[7] Z.J. Wu, A.R. Masri, R.W. Bilger, An experimental investigation of the turbulence structure of a lifted H-2/N-2 jet flame in a vitiated co-flow, Flow Turbul. Combust. 76 (1) (2006) 61–81.
[8] R.L. Gordon, A.R. Masri, E. Mastorakos, Simultaneous rayleigh temperature, OH- and CH_2O-lif imaging of methane jets in a vitiated coflow, Combust. Flame 155 (2008) 181–195.
[9] R.R. Cao, S.B. Pope, A.R. Masri, Turbulent lifted flames in a vitiated coflow investigated using joint PDF calculations, Combust. Flame 142 (4) (2005) 438–453.
[10] F.C. Christo, B.B. Dally, Modeling turbulent reacting jets issuing into a hot and diluted coflow, Combust. Flame 142 (1–2) (2005) 117–129.
[11] S.H. Kim, K.Y. Huh, B. Dally, Conditional moment closure modeling of turbulent nonpremixed combustion in diluted hot coflow, Proc. Combust. Inst. 30 (2005) 751–757.
[12] R.L. Gordon, A.R. Masri, S.B. Pope, G.M. Goldin, A numerical study of auto-ignition in turbulent lifted flames issuing into a vitiated co-flow, Combust. Theory Modell. 11 (3) (2007) 351–376.
[13] P. Domingo, L. Vervisch, D. Veynante, Large-eddy simulation of a lifted methane jet flame in a vitiated coflow, Combust. Flame 152 (3) (2008) 415–432.
[14] S.S. Patwardhan, S. De, K.N. Lakshmisha, B.N. Raghunandan, CMC simulations of lifted turbulent jet flame in a vitiated coflow, Proc. Combust. Inst. 32 (2009) 1705–1712.
[15] S. Kumar, P.J. Paul, H.S. Mukunda, Prediction of flame liftoff height of diffusion/partially premixed jet flames and modeling of mild combustion burners, Combust. Sci. Technol. 179 (2007) 2219–2253.
[16] I.S. Ertesvag, B.F. Magnussen, The eddy dissipation turbulence energy cascade model, Combust. Sci. Technol. 159 (2000) 213–235.
[17] R. Cabra, J.Y. Chen, R.W. Dibble, A.N. Karpetis, R.S. Barlow, Lifted methane–air jet flames in a vitiated coflow, Combust. Flame 143 (4) (2005) 491–506.
[18] K.M. Lyons, Toward an understanding of the stabilization mechanisms of lifted turbulent jet flames: experiments, Prog. Energy Combust. Sci. 33 (2) (2007) 211–231.
[19] L. Vanquickenborne, A. van Tiggelen, The stabilization mechanism of lifted diffusion flames, Combust. Flame 10 (1) (1966) 59–69.
[20] G.T. Kalghatgi, Lift-off heights and visible lengths of vertical turbulent jet diffusion flames in still air, Combust. Sci. Technol. 41 (1) (1984) 17–29.
[21] J. Buckmaster, Edge-flames, Prog. Energy Combust. Sci. 28 (5) (2002) 435–475.
[22] N. Peters, F.A. Williams, Liftoff characteristics of turbulent jet diffusion flames, AIAA J. 21 (3) (1983) 423–429.
[23] R.C. Miake-Lye, J.A. Hammer, Lifted turbulent jet flames: a stability criterion based on the jet large-scale structure, Proc. Combust. Inst. 22 (1988) 817–824.
[24] C.N. Markides, E. Mastorakos, An experimental study of hydrogen autoignition in a turbulent co-flow of heated air, Proc. Combust. Inst. 30 (2005) 883–891.
[25] C.S. Yoo, R. Sankaran, J.H. Chen, Three-dimensional direct numerical simulation of a turbulent lifted hydrogen jet flame in heated coflow: flame stabilization and structure, J. Fluid Mech. 640 (2009) 453–481.
[26] E. Mastorakos, Ignition of turbulent non-premixed flames, Prog. Energy Combust. Sci. 35 (1) (2009) 57–97.
[27] M.J. Tummers, D.M. Passchier, Spectral analysis of biased LDA data, Measur. Sci. Technol. 12 (2001) 1641–1650.

[28] E.H. van Veen, D. Roekaerts, Thermometry for turbulent flames by coherent anti-Stokes Raman spectroscopy with simultaneous referencing to the modeless excitation profile, Appl. Opt. 44 (32) (2005) 6995–7004.
[29] K.M. Lyons, K.A. Watson, C.D. Carter, J.M. Donbar, Upstream islands of flame in lifted-jet partially premixed combustion, Combust. Sci. Technol. 179 (5) (2007) 1029–1037.
[30] I. Boxx, C. Heeger, R. Gordon, B. Bohm, M. Aigner, A. Dreizler, W. Meier, Simultaneous three-component PIV/OH-PLIF measurements of a turbulent lifted, C_3H_8–argon jet diffusion flame at 1.5 kHz repetition rate, Proc. Combust. Inst. 32 (2009) 905–912.
[31] A.R. Masri, R. Cao, S.B. Pope, G.M. Goldin, PDF calculations of turbulent lifted flames of H-2/N-2 fuel issuing into a vitiated co-flow, Combust. Theory Modell. 8 (1) (2004) 1–22.
[32] G.A. Richards, M.M. McMillian, R.S. Gemmen, W.A. Rogers, S.R. Cully, Issues for low-emission, fuel-flexible power systems, Prog. Energy Combust. Sci. 27 (2) (2001) 141–169.
[33] C.J. Montgomery, C.R. Kaplan, E.S. Oran, The effect of coflow velocity on a lifted methane–air jet diffusion flame, Proc. Combust. Inst. 27 (1998) 1175–1182.
[34] E. Mastorakos, T.A. Baritaud, T.J. Poinsot, Numerical simulations of autoignition in turbulent mixing flows, Combust. Flame 109 (1–2) (1997) 198–223.
[35] S. Sreedhara, K.N. Lakshmisha, Autoignition in a non-premixed medium: DNS studies on the effects of three-dimensional turbulence, Proc. Combust. Inst. 29 (2002) 2051–2059.
[36] T. Echekki, J.H. Chen, Direct numerical simulation of autoignition in non-homogeneous hydrogen–air mixtures, Combust. Flame 134 (3) (2003) 169–191.
[37] R.L. Gordon, A.R. Masri, E. Mastorakos, Heat release rate as represented by $[OH] \times [CH_2O]$ and its role in autoignition, Combust. Theory Modell. 13 (4) (2009) 645–670.
[38] S.B. Pope, Turbulent Flows, Cambridge University Press, 2000.